Indian Journal of Radio & Space Physics
Vol. 32, December 2003, pp. 329-336

An improved data reduction technique for the retrieval of the Doppler parameters from interference fringes obtained by a high resolution Fabry-Perot spectrometer

Tarun Kumar Pant[1], R Suhasini [2], S Gurubaran[3] & R Sridharan[1]

[1]Space Physics Laboratory, Thiruvananthpuram 695 022

[2]Nitya Laboratories, Hyderabad (AP) 500 082

[3]Equatorial Geophysical Research Laboratory, Tirunelveli 627 011

Received 31 May 2002; revised 1 April 2003; accepted 11 August 2003

A new data analysis scheme for retrieving Doppler temperatures from high resolution Fabry-Perot spectrometer fringes is described. Important aspects of parametric representation of the instrument function, convolution and the various instrument-broadening functions are discussed in detail. Complete theoretical background highlighting the method for recovering Doppler parameters and involved errors using the instrument-broadened airglow emission profile are provided. Further, a criterion is set to select proper airglow line profiles for the analysis.

Keywords: Doppler parameter, Interference fringes, Fabry-Perot spectrometer, Airglow emission

1 Introduction

Since the first spectroscopic measurements on naturally occurring OI(^{1}D-^{1}S) radiation from the night sky[1], the ground-based spectroscopy entered a new era with the development of spectroscopic instruments of high spectral resolving power and large throughput. Among the various optical techniques available today, the Fabry-Perot (FP) spectrometry has become the instrument of choice for low light level ground-based sensing of the upper atmosphere. Jacquinot[2] established that, out of all the spectroscopic devices where interference of light yields the spectrum, the FP interferometer has the highest luminosity for a given spectral resolution along with the Michelson interferometer. A comprehensive treatise on Fabry-Perot theory has been given by Chabbal[3]. Hernandez[4] further established the usefulness of Fabry-Perot spectrometer by analysing the technical details of the same. The use of the FP spectrometers to determine temperature and winds prevailing in earth's upper atmosphere is now well established, in part, due to the elegant physical principle upon which this experimental technique is based. The measurement of the aforesaid parameters using this technique involves monitoring of the various naturally occurring airglow emission lines in the upper atmosphere. These natural emissions are normally associated with the forbidden electronic transitions of neutral and ionised species[5]. Because of the associated long lifetime with the metastable transition states, the excited species tend to attain thermal equilibrium due to multiple collisions with the surrounding medium before radiation. The distribution of these species is nearly Maxwellian. Therefore, the line profile/Doppler profile of the emitted radiation reflects not only the kinetic temperature of the region from where the emission occurs, in terms of profile width, i.e. Doppler width, but also the bulk motion or the wind in that region in terms of Doppler shift[6]. As the magnitude of the Doppler effects associated with typical wind and temperature existing in the upper atmosphere is small, a spectroscopic device such as a FP spectrometer of very high spectral resolution is necessary for their determination. The FP spectrometers have been used by various research groups[7-10], in India, to study primarily the thermospheric chemistry, thermodynamics and energetics. Most commonly studied emission has been the OI 6300 Å red line originating at ~250 km altitude during nighttime. It has been observed that the average OI 6300 Å intensity levels lie at around 50-100 Rayleigh during nighttime and can even vary by an order of magnitude depending upon the background electron densities in F-region. Systematic measurements on the two thermospheric parameters, namely, temperature and wind have been made since 1986 from Mt.Abu (24.6°N, 72.7°E geogr, 20°N dip lat.) using a central

aperture scanning high resolution FP spectrometer, operating at OI 6300 Å emission[9,11]. The data reduction technique, presented in this paper, was developed and tested using the database obtained by the aforesaid spectrometer. It is fairly well understood that all the components in a spectrometer ranging from FP etalon to the photon detector significantly modify the spectroscopic characteristics of the natural emission lines which are being observed. Therefore, in the case of a FP spectrometer, all the broadening factors and corresponding finesse define its response to any incoming emission. Hence, the determination of a line profile requires to have *a priori* information about two factors: (i) the knowledge of the source under consideration and (ii) a knowledge of the integrated instrument response.

This makes the task of obtaining accurate temperature, wind velocity and emission line intensities difficult by using the interferometric techniques. Therefore, alongwith the ongoing developments in optical technology, a need is felt for a general data analysis scheme with realistic determination of the required parameters and involved errors. In the past, several methods for retrieving the Doppler temperature from measured emission profile have been suggested[3,12]. However, most of these data reduction schemes have a limitation that they work best with only low levels of inherent noise. This paper presents a detailed account of an alternative data reduction scheme for obtaining the Doppler temperature from the FP fringes. This scheme is more general in its use. Details regarding the important aspects of FP etalon in spectrometer functioning that has relevance in the formulation of the present scheme, can be obtained from available studies[3,4].

2 Retrieval of Doppler parameters from observed interference fringes

As mentioned earlier, during actual observations, the output profile is the original source profile convolved with the finite bandpass of the FP spectrometer. In other words, all the instrument-broadening functions get superimposed on the source width and the final result is a broadened representation of the original intensity distribution. The output profile, therefore, is expressed as a convolution of the source profile with the instrument function, i.e.

$$EO(x)=\int I(x-x')\times S(x')\mathrm{d}x' \qquad \ldots (1)$$

where, $EO(x)$ is the expected output profile, $I(x)$ the instrument broadening function and $S(x)$ the source function.

The effect of various factors contributing to broadening due to the instrument has been explained by many workers[3,12]. However, in actual observations the intensity of the signal is contaminated by inherent noise, the background continuum from sky and contributions from neighbouring spectral lines present in the medium being observed, if any. So the actual observed profile $O(x)$ is given as

$$O(x)=EO(x)+\varepsilon(x)+B \qquad \ldots (2)$$

where, $\varepsilon(x)$ and B are the noise and background continuum, respectively.

Therefore, in order to retrieve the Doppler parameters, the source function $S(x)$ is to be obtained first, from the observed, convolved nightglow intensity profile. It is clear from the convolution integral [Eq. (1)], that one obvious way to obtain the source function $S(x)$ would be to go for a deconvolution process in the Fourier domain. But, for signals having inherent noise, this process of deconvolution becomes ill conditioned and hence cannot reproduce the source function without adding some side effects[13]. The above aspects of a deconvolution approach has also been confirmed by Anandarao and Suhasini[14]. Therefore, the present method to retrieve the Doppler parameter was developed taking into account not only the noise inherent in the signal, but also the various possible limitations faced during the observations.

3 Spectral line shape

In the upper atmosphere, the intensity distribution of the airglow at a certain wavelength, under thermal equilibrium at temperature T_n is represented by the Gaussian distribution as

$$I(\lambda)=\frac{I_0}{\mathrm{d}\lambda}\exp\left[-\frac{(\lambda-\lambda_0)^2}{\mathrm{d}\lambda^2}\right] \qquad \ldots (3)$$

This Gaussian distribution is centered about λ_0 and the width of the Gaussian distribution ($\mathrm{d}\lambda$) arises because of the distribution of velocities of atoms contributing towards the particular spectral emission. The Doppler width of the emission profile is related to the full width at half maximum ($\delta\lambda$) by

$$\delta\lambda=\left(2\sqrt{\ln 2}\right)d\lambda \quad \ldots (4)$$

and to the kinetic temperature (T_n) by

$$\frac{\delta\lambda}{\lambda}=\left(7.16\times10^{-7}\sqrt{\frac{T_n}{M}}\right) \quad \ldots (5)$$

where M is the molecular/atomic weight of the emitting species in atomic mass units (amu). The same (Gaussian) emission line profile as observed by the FP spectrometer could also be written as

$$EO(X_i,P_j)=\sum_{k=1}^{n} I(X_i,X_k)\,S(X_k,P_j) \quad \ldots (6)$$

The functions $EO(X_i,P_j)$, $I(X_i,X_k)$ and $S(X_k,P_j)$ are the expected output profile, instrument function, and the source function, respectively. The above expression represents the scanning of interference fringes [the data taken in terms of discrete steps in the parameter X_i, i.e. pressure in the present case]. In this scanning technique, the net result of a scan over a free spectral range is a set of sample points. The parameters of the Doppler profile to be determined are P_j's, i.e. P_1, P_2, P_3 which are the peak line intensity, the line center and the line width, respectively. In terms of P_1, P_2, P_3 (the required parameters) the source profile becomes:

$$S(X_k,P_j)=\frac{P_1}{P_3}\exp\left[-\frac{(X_k-P_2)^2}{P_3^2}\right] \quad \ldots (7)$$

3.1 Determination of P_j's

Since the form of the expected output profile $EO(X_i,P_j)$ is known, an approach of linearizing the fitted curve function $EO(X_i,P_j)$ in the parameter-space close to the optimum values of P_j' is adopted for the determination of these parameters[15,16]. The linearization process uses the results of linear least squares which is an iterative procedure based on Taylor series expansion about the approximated required solution of P_j'. As the first step, the profile function $EO(X_i,P_j)$ is expanded in a Taylor series about P_j' (a set of initial approximate solutions).

$$EO(X_i,P_j)=EO(X_i,P_j^0)+\sum\left(\left(\frac{\partial EO(X_i,P_j^0)}{\partial P_j}\right)\right)_i P_j' \quad \ldots (8)$$

where,

$$P_j=P_j^0+P_j' \quad \ldots (9)$$

and

$$EO=EO(X_i,P_j^0) \quad \ldots (10)$$

The higher order dependence of P_j' is neglected in the Taylor expansion. The initial value of P_j' s correspond to the observed profile $O(X_i)$ assuming it to follow Gaussian distribution. Sum of the squares of deviation (χ^2) becomes:

$$\chi^2=\sum_{i=1}^{n} W_i\left[O(X_i)-EO(X_i,P_j^0)\right]^2 \quad \ldots (11)$$

Minimization of the above term would lead to three equations which are to be solved for P_j'. The weights W_i are the reciprocal of the intensity counts at each P_j. Thus found P_j's, give the estimate of the parameters to be used as initial value for the next iteration. In the present case, the convolved output or the Doppler-broadened profile is given by

$$EO(X_i,P_j)=\sum_{k=1}^{n} I(X_i-X_k)\left[\frac{P_1}{P_3}\exp\left(-\frac{(X_k-P_2)^2}{P_3^2}\right)\right] \quad \ldots (12)$$

For the minimization of sum squares of deviation, the deviations with respect to P_j' should be zero, i.e.

$$\frac{\partial}{\partial P_k'}\left[\sum_{i=1}^{n} W_i \times\left\{O(X_i)-EO(X_i,P_j^0)-\sum_{j=1}^{3}\left(\frac{\partial EO(X_i,P_j^0)}{\partial P_j}\right)_i P_j'\right\}^2=0\right] \quad \ldots (13)$$

and

$$2\times\left[\sum_{i=1}^{n} W_i\left\{O(X_i)-EO(X_i,P_j^0)-\sum_{j=1}^{3}\left(\left(\frac{\partial EO(X_i,P_j^0)}{\partial P_j}\right)\right)_i P_j'\right\}\right] \times\left(\frac{\partial EO(X_i,P_j^0)}{\partial P_k'}\right)_i=0 \quad \ldots (14)$$

The second and higher order derivatives are neglected. However, the derivatives are

$$\frac{\partial EO(X_i,P_j)}{\partial P_1}=\frac{EO(X_i,P_j)}{P_1} \quad \ldots (15)$$

$$\frac{\partial EO(X_i,P_j)}{\partial P_2}=\frac{2(X_k-P_2)}{P_3^2}EO(X_i,P_j) \quad \ldots (16)$$

$$\frac{\partial EO(X_i,P_j)}{\partial P_3}=\left[\frac{2(X_k-P_2)}{P_3^2}-\frac{1}{P_3}\right]EO(X_i,P_j) \quad \ldots (17)$$

$$\sum_{i=1}^{n} W_i O(X_i)\left(\frac{\partial EO(X_i,P_j^0)}{\partial P_k'}\right)_i - \sum_{i=1}^{n} W_i EO(X_i,P_j^0)\left(\frac{\partial EO(X_i,P_j^0)}{\partial P_k'}\right)_i - \sum_{i=1}^{n}\sum_{j=1}^{3} W_i\left(\frac{\partial EO(X_i,P_j^0)}{\partial P_j'}\right)_i\left(\frac{\partial EO(X_i,P_j^0)}{\partial P_k'}\right)_i P_j'=0 \quad \ldots (18)$$

Equation (18) provides the normal equation.

The important thing here is, that, the derivatives $\frac{\partial EO(X_i,P_j^0)}{\partial P_k'}$ are numbers and the Eq. (18) gives a set of simultaneous equations to be solved for P_1, P_2, P_3. If

$$\sum_{i=1}^{n} W_i O(X_i)\left(\frac{\partial EO(X_i,P_j^0)}{\partial P_k^0}\right)_i - \sum_{i=1}^{n} W_i EO(X_i,P_j^0)\left(\frac{\partial EO(X_i,P_j^0)}{\partial P_k^0}\right)_i = C_k \quad \ldots (19)$$

The normal equation [Eq. (18)] becomes

$$C_k - \sum_{i=1}^{n} W_i\left(\left(\frac{\partial EO(X_i,P_j)}{\partial P_j}\right)_i\left(\frac{\partial EO(X_i,P_j)}{\partial P_k}\right)_i P_k'\right)=0 \quad \ldots (20)$$

So,

$$C_1=\sum_{i=1}^{n} W_i\left[\left(\frac{\partial EO(X_i,P_j)}{\partial P_1^0}\right)_i+\left(\frac{\partial EO(X_i,P_j)}{\partial P_2^0}\right)_i + \left(\frac{\partial EO(X_i,P_j)}{\partial P_3^0}\right)_i\right]\left(\frac{\partial EO(X_i,P_j)}{\partial P_1^0}\right)_i P_k' \quad \ldots (21)$$

Similar solutions for k= 1, 2, 3 can be written as

$$C_1=A_{11}P_1+A_{12}P_2+A_{13}P_3 \quad \ldots (22)$$

$$C_2=A_{21}P_1+A_{22}P_2+A_{23}P_3 \quad \ldots (23)$$

$$C_3=A_{31}P_1+A_{32}P_2+A_{33}P_3 \quad \ldots (24)$$

Or, in matrix form, the above equation can be written as

$$\begin{pmatrix} C_1 \\ C_2 \\ C_3 \end{pmatrix}=\begin{pmatrix} A_{11} & A_{12} & A_{13} \\ A_{21} & A_{22} & A_{23} \\ A_{31} & A_{32} & A_{33} \end{pmatrix}\begin{pmatrix} P_1 \\ P_2 \\ P_3 \end{pmatrix} \quad \ldots (25)$$

In other words,

$$C=A\times P \quad \ldots (26)$$

where, C, A and P are general terms used for the above mentioned matrices. To obtain P, we used matrix inversion technique,

$$P=A^{-1}\times C \quad \ldots (27)$$

and the estimates of P_j's are obtained by adopting Gauss-Jordan elimination process for coefficient matrix A^{-1}. The parameters P_j's, thus estimated, serve as the initial values for the next iteration, and the whole procedure is repeated till the solution converges, providing the final output, i.e. the peak profile intensity, peak position and the profile width. The profile width provides the temperature and, once the peak position of the fringe is determined, the line-of-sight velocity is obtained using the Doppler relationship

$$v=c\times\frac{\delta\lambda}{\lambda} \quad \ldots (28)$$

where, c is the velocity of light and $\delta\lambda$ is the change in the peak position of the fringe from emission wavelength λ (no Doppler shift/reference). The parameter v is the mean velocity of the emitting species along the line-of-sight of the instrument. The reference wavelength is obtained using the laboratory He-Ne laser source at known wavelength 6328Å. In the present case, the narrow band (3Å) interference filter is temperature-tuned for maximum transmission at 6300Å for the O^1D emission. The filter temperature tuned to the peak transmission is maintained to an accuracy of 0.5°C. Further, it must be mentioned that, in the present case, the Doppler velocity thus derived is only the line-of-sight velocity which, in fact, is a component of the overall wind flow along the meridian. Therefore, knowing the elevation of the viewing angle for the instrument at a given experimental location would enable one to estimate the meridional wind velocity. The inference whether the wind is equatorward or poleward is drawn on the basis of the spectroscopically measured shift in the atmospheric emission, i.e. shift towards longer wavelength would mean equatorward wind, while poleward wind corresponds to shifts towards smaller wavelength when the spectrometer is pointing north. An average of the line profiles obtained from the zenith directions has already been shown to be a good reference for wind estimations by earlier workers[17]. In the present case also, a few good zenith profiles are taken every night and the average peak position serves as the reference for estimating the wavelength shift mentioned above.

The Doppler temperatures and winds at thermospheric heights for one night derived from observed airglow profiles using the present data reduction scheme are shown, as examples, in Fig. 1.

3.2 Noise reduction and estimation of background

All the data points observed during a scan consist of the desired signal and some superimposed noise, which is random in nature and causes the errors in the determination of final temperature. Figure 2 clearly shows the steep increase in the standard deviation in temperature estimation with low signal strengths. However, the frequency spectrum of the noise is rather flat compared to that of the fringe peak[18]. The intensity fluctuations in the detection process during a real time observation follow Poisson distribution[4,16]. The importance of uncertainties in measurements in real time conditions is highlighted and quantified in a series of studies[19-21]. Hays and Roble[18] have clearly shown that the Fourier decomposition technique can efficiently filter out the high frequency component, i.e. noise from the incoming signal photon fields by using only the first five coefficients.

The present data reduction scheme also adopts the

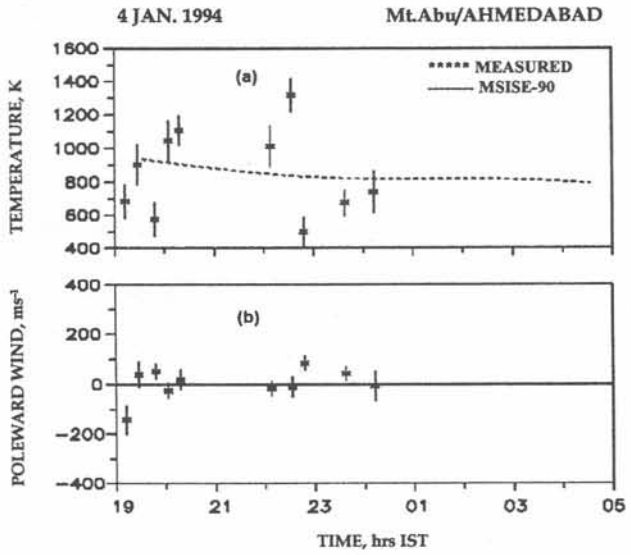

Fig. 1—Sample results showing the temporal variation of the spectroscopically measured F-region Doppler temperature (a) and line-of-sight winds (b). [These parameters were obtained using the proposed data analysis technique. The curve presented by MSISE-90 denotes the thermospheric model (MSISE-90) predicted thermospheric temperature for given geophysical conditions.]

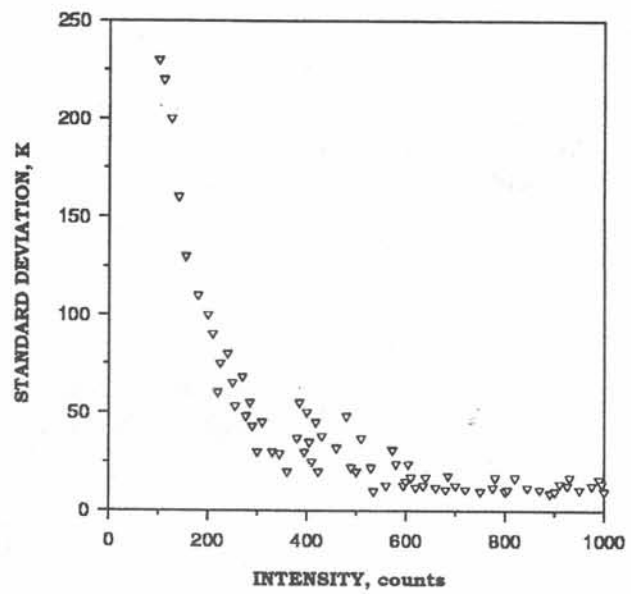

Fig. 2—Plot of the 1σ error on the temperature determination as a function of the observed airglow intensity [The error drastically increases when the source becomes faint.]

Fourier decomposition technique to minimize the random errors associated with photon noise. The airglow profile which is a function of pressure (wavelength) and is Gaussian in shape, can mathematically be written as the superposition of even (cosine functions) and odd (sine) functions of various orders (m). If $Y_s(x)$ is the actual airglow profile, then in terms of Fourier components it can be written as

$$Y_s(X)=\frac{Y_{co}}{2}+\sum Y_m \cos(mX+\alpha) \quad \ldots (29)$$

here Y_{co} is the zeroth order transform of the data. In the present analysis, $m = 4$ is the limit for coefficient order, as explained above. The amplitude defined by $\sqrt{\{(Y_{cm})^2 + (Y_{sm})^2\}}$ and α as $\tan^{-1}(Y_{sm}/Y_{cm})$ are the odd and even (sine and cosine) Fourier transform of the data. This method enables us to treat the data free of inherent random noise. However, there remains one more component of noise to be removed from the observed data, i.e. in the form of background continuum.

There is no qualitative definition, describing the background, but the lowering of contrast in observed profiles is associated with the presence of background radiation during observations. It has been shown by Chabbal[3] that the observed contrast (C_{act}) of the airglow profile is always less than the instrument contrast (C) and is related to the product of the instrument contrast and the transmission of the etalon (τ). He also gave a theoretical response curve[3] for the instrument as the variation of transmission for the etalon for different source width(s) compared to etalon widths (E), where the transmission actually is

$$\tau = \frac{C_{act}}{C} \quad \ldots (30)$$

where, C is the resultant contrast for an ideal monochromatic source (zero width) and C_{act} the contrast for assumed source widths. The observed contrast C_{act} is given by

$$C_{act}=\frac{I_{max}-BG}{I_{min}-BG} \quad \ldots (31)$$

where, I_{max}, I_{min}, and BG represent the maximum, minimum and background intensity levels, respectively. Using Eqs (30), (31) and the transmission curve, the background can be estimated for any source (i.e. source widths under consideration). In the present data reduction scheme, the BG is iteratively estimated for each step of parameter fitting. The estimated background is subtracted from the observed data and then the profile is subjected to the analysis for determination of the Doppler parameters. Figure 3 shows the deconvolved airglow profile after applying the Fourier decomposition technique for noise reduction and due correction for the background. A theoretical profile determined for the estimated temperature from the former profile is also shown for comparison.

3.3 Estimation of errors in the evaluation of Doppler parameters

Owing to the nature of the distribution of observed photons and inherent noise in the present measurements, the uncertainty associated with the determination of P_j parameters is the root sum square of the products of the standard deviation of each data point σ_i multiplied by the effect that the data point has on its determination[16], i.e.

$$\sigma_{P_j}^2 = \sum_{i=1}^{n}\left(\sigma_i^2\left\{\frac{\partial P_j}{\partial OX_i}\right\}^2\right) \quad \ldots (32)$$

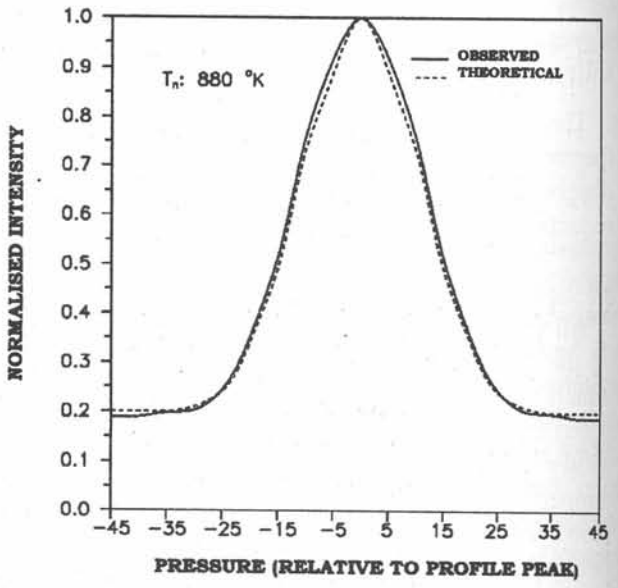

Fig. 3—Deconvolved airglow profile after applying the Fourier decomposition technique for noise reduction and due correction for the background

reduce the airglow intensity levels leading to low signal-to-noise ratio. At the same time, very low levels of airglow intensity itself have significant noise merged in the signal, which yields a very low signal-to-noise ratio, not adequate enough to obtain reliable Doppler temperatures and winds[17]. The thermal stabilization of the FP etalon would also be of great importance, especially, in spectrometers where variation of refractive index is used for scanning the wavelength. Any non-linearity in the change of refractive index (μ), over the pressure range used for the scanning would also lead to distortions in the profile. In present case, this non-linearity is insignificant (10^{-3}). Similarly, the linearity in the temperature dependence of μ (refractive index) must also be ensured. In the present case, we maintain the thermal stability of the etalon to a level higher than 0.1°C during the scan, and to an extent of 0.5°C throughout the night. Along with this, the profiles with drastic changes in intensity are not included for the estimation of Doppler parameters to avoid any ambiguity. In a similar way, severely distorted profiles, irrespective of the cause, need to be screened out and are not included in the analysis. Further, the present analysis procedure applies to Doppler-broadened emission lines that are free from the contribution of the overlapping orders of nearby emissions. However, the presence of such contaminations would severely affect the final temperatures. Nevertheless, a proper instrument design and appropriate selection of filters, more sophisticated scanning techniques and detectors would minimize their effect on the estimation of the temperature and winds. For instance, the use of multiple etalon systems will reduce the background and increase the contrast ratio significantly[24]. Similarly, detectors with higher sensitivity in specific wavelength regions would enhance the signal-to-noise ratios for a given spectrometer. Unlike the pressure scanning technique employed in the present study, use of piezo-electric servo controlled etalons will provide better scan resolution and higher fringe stability. These factors would significantly improve the quality of the airglow data.

Acknowledgements

This work is supported by the Department of Space, Govt. of India.

References

1 Babcock H D, *Astrophys J (USA)*, 57 (1923) 209.
2 Jacquinot P, *J Opt Soc (USA)*, 44 (1954) 761.
3 Chabbal R, *J Rech Atmos (France)*, 24 (1953) 138.
4 Hernandez G, *Fabry Perot interferometers* (Cambridge Univ. Press, Cambridge), 1953.
5 Chamberlain J W, *Physics of the Aurora and Airglow* (Academic Press, New York), 1961.
6 Hernandez G & Killeen T L, *Adv Space Res (UK)*, 8 (1988) 149.
7 Rajaraman T N, *Optical studies in the upper atmosphere*, Ph D Thesis, Gujarat University, 1982.
8 Desai J N, *Proc Indian Acad Sci*, 93 (1984) 189.
9 Gurubaran S, *Investigation of low latitude thermosphere-ionosphere system*, Ph D Thesis, Gujarat University, 1988.
10 Sastri J H & Rao H N R, *J Atmos & Terr Phys (UK)*, 56 (1988) 775.
11 Pant Tarun K, *Study of the thermosphere ionosphere coupling under varying geophysical conditions*, Ph D Thesis, Gujarat University, 1998.
12 Turgeon E C & Shepherd G G, *Planet & Space Sci (UK)*, 32 (1962) 295.
13 Cooper M J, *Phys Bull (UK)*, Oct issue, 1977, 463.
14 Anandarao B G & Suhasini R, *Bull Astron Soc India*, 14 (1985) 34.
15 Draper N R & Smith H, *Applied Regression Analysis* (John Wiley and Sons Inc., New York), 1966.
16 Bevington P R, *Data Reduction and Error Analysis for the Physical Sciences* (McGraw-Hill Book Co, New York) 1969.
17 Hernandez G & Roble R G, *J Geophys Res (USA)*, 81 (1976) 2065.
18 Hays P B & Roble R G, *Appl Opt (USA)*, 10 (1971) 193.
19 Hernandez G & Roble R G, *Appl Opt (USA)*, 18 (1979) 3376.
20 Hernandez G, *Appl Opt (USA)*, 1 (1982) 1695.
21 Hernandez G, *Appl Opt (USA)*, 24 (1985) 2442.
22 Sridharan R, Gurubaran S, Raghavarao R & Suhasini R, *J Atmos & Terr Phys (UK)*, 33 (1991) 575.
23 Pant Tarun K & Sridharan R, *Ann Geophys (France)*, 16 (1998) 1513.
24 Barmore F E, *Planet & Space Sci (UK)*, 25 (1977) 185.